Effect of amorphous SiO_2 matrix on structural and magnetic properties of $Cu_{0.6}Co_{0.4}Fe_2O_4/SiO_2$ nanocomposites

Thomas Dippong [a, *], Erika Andrea Levei [b], Oana Cadar [b], Iosif Grigore Deac [c], Mihaela Lazar [d], Gheorghe Borodi [d], Ioan Petean [e]

[a] Technical University of Cluj-Napoca, Department of Chemistry and Biology, 76 Victoriei Street, 430122, Baia Mare, Romania
[b] INCDO-INOE 2000, Research Institute for Analytical Instrumentation, 67 Donath Street, 400293, Cluj-Napoca, Romania
[c] Babes-Bolyai University, Faculty of Physics, 1 Kogalniceanu Street, 400084, Cluj-Napoca, Romania
[d] National Institute for Research and Development of Isotopic and Molecular Technologies, 65-103 Donath Street, 400293, Cluj-Napoca, Romania
[e] Babes-Bolyai University, Faculty of Chemistry and Chemical Engineering, 11 Arany Janos Street, 400028, Cluj-Napoca, Romania

ARTICLE INFO

ABSTRACT

This study presents the structural and magnetic characterization of $\alpha Cu_{0.6}Co_{0.4}Fe_2O_4/(100-\alpha)SiO_2$ ($\alpha = 0$, 25, 50, 75 and 100%) nanocomposites prepared by sol-gel method, followed by thermal treatment at 200, 500, 800 and 1200 °C. The SiO_2 matrix was found to be amorphous. At low ferrite contents, the obtained Cu−Co ferrite is unpurified by crystalline CoO, while at high ferrite contents single-phase Cu−Co ferrite is obtained. The particle sizes increase from 30 to 120 nm with increasing ferrite content embedded in the SiO_2 matrix, while the crystallinity increases at higher thermal treatment temperature. The atomic force microscopy revealed the morphology of the $Cu_{0.6}Co_{0.4}Fe_2O_4/SiO_2$ nanocomposites. For samples treated at 200 and 500 °C, the specific surface area increases and the crystallinity decreases with increasing SiO_2 content. For all samples, the surface area decreases with the increasing annealing temperature. The SiO_2 matrix is diamagnetic and does not show hysteresis curve. The saturation magnetization and remanent magnetization improved, while the coercivity and magnetic anisotropy decreased with increasing Cu−Co ferrite content embedded in SiO_2 matrix.

© 2020 Elsevier B.V. All rights reserved.

1. Introduction

In recent years, Cu−Co ferrites received a great interest due to the wide diversity of magnetic, electronic and dielectric properties. These properties are highly sensitive to cation distribution among tetrahedral and octahedral sites, to SiO_2: ferrite ratio, to substitution degree between divalent ions and to thermal treatment [1−3]. The tunable structural and magnetic properties of Cu−Co ferrites make them suitable candidates for applications in catalysis, wastewater treatments, ferrofluids, microwaves devices, high frequency integrated inductors, data storage, resonance imaging, hybrid supercapacitors, transformer cores, chock coils, noise filters, computer circuitry, communication and medicine [4−10]. The high surface-to-volume ratio of nanoparticles results in a large number of atoms, that are less stable compared to bulk atoms. This make the nanomaterial's surface more reactive, resulting in enhanced or new properties (*i.e.* mechanical strength, better conductivity) compared to bulk materials. The coordination number of surface atoms is lower than of core atoms, leading to various surface effects such as spin canting, spin disorder and dead magnetic layer. In magnetic nano-ferrite systems, the size, morphology and magnetic properties are highly interrelated [10]. Thus, the required coercivity (H_C) and saturation magnetization (M_S) can be achieved by customizing the chemical composition, size and morphology of the nanoparticles [4]. The thermal treatment allows the tailoring of ferromagnetic resonance and of permeability at low frequencies and low alternating magnetic field [5,9,10]. $CoFe_2O_4$ is a ferromagnetic nanomaterial with high anisotropy constant (K), H_C and Curie temperature, moderate M_S, excellent chemical and mechanical stability, large magnetostrictive coefficient and high electrical resistance [2,10−12].

Generally, the synthesis of ferrites can be achieved by sol-gel, hydrothermal, solvothermal, co-precipitation, spray hydrolysis, organometallic compounds decomposition, solid-state reaction, microwave, microemulsion, high-energy ball-milling and

---

* Corresponding author.
E-mail address: dippong.thomas@yahoo.ro (T. Dippong).

mechanical alloying methods [1–6]. The sol-gel route is one of the most advantageous method for the preparation of nanocomposites as it proves to be a simple, low-cost method that allows good control of the reaction product structure, homogeneity, physico-chemical and surface properties [1–4,13–15]. The major drawback of the sol-gel method is the obtaining of various crystalline and/or amorphous phases and irregularly-shaped nanoparticles due to the large quantity of gas evolved during the decomposition of the organic solvents and the distribution of viscous sol into nanopores only by weak capillary forces [1–5].

Recently, the embedding of magnetic ferrites in SiO_2 received considerable attention due to the possibility to obtain nano-materials with different properties than of that of non-embedded ferrite, as the SiO_2 network acts as a buffer and limits the nano-particles agglomeration and minimize the surface roughness and spin disorder at room temperature, increasing the H_C of $CoFe_2O_4/SiO_2$ compared to that of $CoFe_2O_4$ [7,11,12].

Previous studies revealed that the structural, morphological and magnetic properties of $Co_xFe_{2-x}O_4$ embedded in SiO_2 matrix de-pends on the annealing temperature and of Co to Fe ratio [16,17]. This dependence was also observed in the case of mixed Co–Ni and Co–Zn ferrites embedded in SiO_2 matrix [18,19].

The aim of the paper is to demonstrate that structural and magnetic properties of $\alpha Cu_{0.6}Co_{0.4}Fe_2O_4/(100-\alpha)SiO_2$ nano-composites (NCs) obtained by sol-gel synthesis followed by annealing at different temperatures depend not only on the ferrite type, synthesis method and annealing temperature, but also on the matrix material and ferrite to matrix ratio. The influence of the ferrite content embedded in the amorphous SiO_2 matrix on struc-tural and morphological properties was investigated by X-ray diffraction (XRD) and atomic force microscopy (AFM), while the formation of the ferrite and SiO_2 matrix was monitored by Fourier-transform infrared spectroscopy (FT-IR). The N_2 adsorption-desorption isotherms were used to determine the specific surface area (SSA) and porosity of the NCs, while the saturation magneti-zation (M_S), coercive field (H_C) and anisotropy constant (K) were determined by vibrating-sample magnetometry.

2. Materials and methods

The $\alpha Cu_{0.6}Co_{0.4}Fe_2O_4/(100-\alpha)SiO_2$ ($\alpha = 0, 25, 50, 75$ and 100%) were prepared by sol-gel method followed by thermal treatment. Copper nitrate ($Cu(NO_3)_2 \cdot 3H_2O$), cobalt nitrate ($Co(NO_3)_2 \cdot 6H_2O$) and ferric nitrate ($Fe(NO_3)_3 \cdot 9H_2O$) were dissolved in 1,4-butanediol (BD) in a molar ratio of 0.6: 0.4: 2: 8. To the nitrate-diol mixture, an ethanolic solution of tetraethyl orthosilicate (TEOS) acidified to pH = 2 using nitric acid, was added drop-wise, under continuous stirring, using an NO_3^-:TEOS molar ratio of 0:2 ($\alpha = 0\%$), 0.5:1.5 ($\alpha = 25\%$), 1:1 ($\alpha = 50\%$), 1.5:0.5 ($\alpha = 75\%$) and 2:0 ($\alpha = 100\%$). The mixture was continuously stirred for 30 min and then exposed to open air for slow gelation. After 6 weeks, the glassy gels were grinded and dried at 200 °C for 5 h, then thermally treated at at-mospheric pressure, in air, at 500, 800 and 1200 °C for 5 h in a LT9 muffle furnace (Nabertherm).

The chemical changes during thermal treatment were investi-gated through the formation and decomposition of functional groups using a Spectrum BX II (PerkinElmer) Fourier-transform infrared spectrometer on KBr pellets containing 1% sample. The X-ray diffraction pattern was recorded at room temperature, using a D8 Advance (Bruker) diffractometer, operating at 40 kV and 40 mA with CuKα radiation ($\lambda = 1.54060$ Å). A JEOL JSPM 4210 Scanning Probe Microscope driven in tapping mode using NSC 15 probes (Mikromasch) at 325 kHz resonant frequency, 40 N/m force constant and 10° tip radius was used for the AFM imaging. The NC's film was prepared by vertical adsorption on glass slides from an

aqueous dispersion of 2.5 g NCs in 10 mL ultrapure water, followed by natural drying and then was tapped by the AFM cantilever to obtain the topographic images at different scan sizes. The optimum view of the adsorbed nano-particles film at an area of 1 μm × 1 μm. AI images were processed in the standard manner using the JEOL WinSPM 2.0 processing soft which allows measuring of nano-particles size, thin film roughness and surface height. The iso-therms were recorded on a Sorptomatic 1990 (Thermo Fisher Scientific) instrument on samples degassed at 200 °C and 2 Pa for 4 h. No pressure variation was observed during 1 h at the end of the degassing process. N_2 adsorption-desorption isotherms measured at −196 °C were used to calculate the specific surface area (SSA) and porosity parameters. The SSA was estimated using the Brunauer, Emmett and Teller equation from the linear section of isotherms ($0.1 < p/p_0 < 0.3$), while the pore size distribution was calculated form the desorption branch of the isotherm using the Dollimore Heal model. The magnetic measurements were performed with a cryogen free VSM magnetometer (CFM- 12 T, Cryogenic Ltd.). The M_S were measured in high magnetic field up to 10 T, while the magnetic hysteresis loops were recorded between −2 and 2 T, at 300 K. The powder samples were embedded in an epoxy resin matrix in order to avoid the displacement of particles.

3. Results and discussion

The XRD patterns and FT-IR spectra of $(Cu_{0.6}Co_{0.4}Fe_2O_4)_\alpha(SiO_2)_{100-\alpha}$ ($\alpha = 0, 25, 50, 75, 100\%$) thermally treated at 200, 500, 800 and 1200 °C are shown in Fig. 1. For $\alpha = 0\%$ (SiO_2), at all tem-peratures, the formation of amorphous SiO_2 matrix is confirmed by the large halo in the 2θ range of 15–30°. Generally, high SiO_2 content and low annealing temperature leads to amorphous NCs. For $\alpha = 25\%$, below 800 °C, the existence of the halo between 15 and 30° suggests an amorphous phase, while at higher temperatures CuO (JCPDS card no. 89-5895 [20]) and $Cu_{0.6}Co_{0.4}Fe_2O_4$ ($CuFe_2O_4$, JCPDS card no. 73-2315 [20]) and $CoFe_2O_4$, JCPDS card no. 02-1045 [20]) starts to form. For $\alpha = 50\%$, at 200 °C the crystallization degree of Cu–Co ferrite increases and CuO appears. The presence of CuO is observed in case of $\alpha = 50\%$ at every thermal treatment. For $\alpha = 75\%$ and $\alpha = 100\%$, at all temperatures, the presence of $Cu_{0.6}Co_{0.4}Fe_2O_4$ as single phase is remarked. The diffraction peaks of $Cu_{0.6}Co_{0.4}Fe_2O_4$ can be attributed to the crystalline phase of spinel ferrite (111), (220), (311), (222), (400), (422), (511) and (440) that crys-tallize in body-centered tetragonal structure, with a space group I41/amd [2,11]. The non-embedded $Cu_{0.6}Co_{0.4}Fe_2O_4$ is highly crys-talline and does not show any impurities even at low temperatures (200 °C), indicating that the oxidic system is formed at this tem-perature. The low intensity, broadened diffraction peaks of NC with low ferrite content indicate the low crystallinity of the NCs, prob-ably due to smaller crystallite size [10,11]. The average crystallite size (D_C) of the samples calculated using the Debye-Scherrer for-mula range between 34 and 110 nm (Table 1) [16–19].

The crystallite size increases with increasing $Cu_{0.6}Co_{0.4}Fe_2O_4$ content in the amorphous SiO_2 matrix and the annealing temper-ature, probably due to the grain growth blocking effect of the ma-trix [1,15–18]. The surface dipole interactions, high surface energy and tension, together with the cation charge distribution within the nanocrystallite induces the shrinking of the lattice, which further determine the drop of the lattice parameter and thus blocks the grain growth [10]. The intensity of diffraction lines increases at high annealing temperatures, due to the high degree of crystallinity and low effects of inert surface layer of the crystals [16–19]. The NCs with low ferrite content contain both crystalline and amorphous phases. The amorphous SiO_2 phase gives a diffraction halo at 2θ between 15 and 40° and is proportional with the area under the diffraction halo, while the crystalline content is proportional with
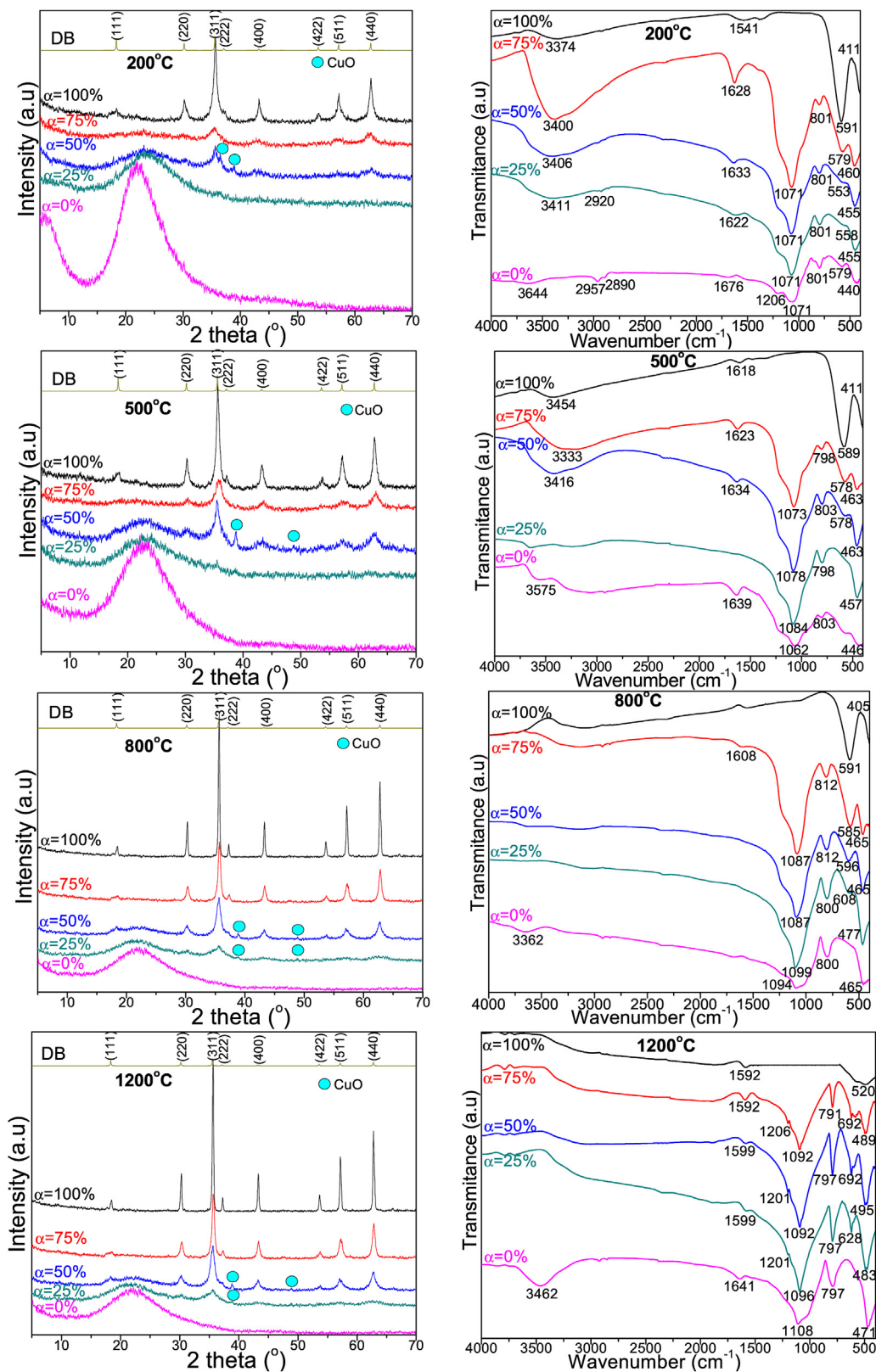
Fig. 1. XRD patterns and FT-IR spectra and of $(Cu_{0.6}Co_{0.4}Fe_2O_4)_\alpha(SiO_2)_{100-\alpha}$ thermally treated at 200, 500, 800, 1200 °C.

the sum of area under all diffraction peaks. The degree of crystallinity is the ratio between the area of all diffraction peaks and the total area for the diffraction peaks and amorphous halo.

The symmetry of different sites occupied by atoms in the crystal lattice determines the vibrational modes present in the samples and thus allows the identification of its structure [21]. Fig. 1 shows

the FT-IR spectra of $(Cu_{0.6}Co_{0.4}Fe_2O_4)_{\alpha}(SiO_2)_{100-\alpha}$ ($\alpha = 0, 25, 50, 75$ and 100%). At low temperatures (200 and 500 °C), the bands around 3333-3644 cm^{-1} are attributed to O−H stretching in Si−OH resulted from the hydrolysis of −Si(OC$_2$H$_5$)$_4$ and in free water molecules. In samples with high SiO$_2$ content, thermally treated at 200 °C, the bands at 2920−2957 and 2890 cm^{-1} are attributed to the asymmetric and symmetric stretching vibration of the C−H bond in −Si(OC$_2$H$_5$)$_4$ structure [15−17].

At all annealing temperatures, the O−H in-plane and out-of-plane bonds appears at 1539-1676 cm^{-1} indicating that the water molecules are chemically adsorbed on the nanoparticles during synthesis [4,16,17,21]. The formation of SiO$_2$ matrix is indicated by the vibration bands of Si−O bond (440-463 cm^{-1}), cyclic Si−O−Si bonds (553-628 cm^{-1}), of Si−O−Si chains (791-812 cm^{-1} and 1062-1108 cm^{-1}) [16−19]. These bands are missing in the non-embedded Cu$_{0.6}$Co$_{0.4}$Fe$_2$O$_4$ ($\alpha = 100$%) where only the presence of the absorption band around 520-692 cm^{-1} attributed to Cu−O and Co−O vibration, and around 405-411 cm^{-1} attributed to Fe−O bonds vibration are observed [16]. Except the SiO$_2$matrix ($\alpha = 0$), all the samples thermally treated at 1200 °C contain M-O absorption bands around 1200 cm^{-1} indicating the presence of Co−O, Cu−O and Fe−O vibrations [15−19].

The two-dimensional topographic images of Cu$_{0.6}$Co$_{0.4}$Fe$_2$O$_4)_{\alpha}(SiO_2)_{100-\alpha}$ thermally treated at 500, 800 and 1200 °C are presented in Fig. 2. The particle size increase with increasing annealing temperature, the smallest particles were obtained for the samples thermally treated at 500 °C, while the biggest for the samples thermally treated at 1200 °C. The nanoparticle size increases also with the increase of the ferrite to SiO$_2$ ratio. The amorphous SiO$_2$ matrix embeds the crystalline ferrite cores resulting multidomenial nanoparticles. Thus, the nanoparticles size estimated by AFM (Table 2) is slightly higher than the crystallite size estimated by XRD (Table 1), indicating that the variation of the amorphous SiO$_2$ content is an important process parameter which allows the control of spreading of the ferrite magnetic domains.

The shape and size of the nanoparticles influences the topography of the adsorbed nanoparticle film on solid substrate (Fig. 3). The surface particularities such as roughness and height are also given in Table 2.

The SiO$_2$ matrix ($\alpha = 0$%) presents small and round nanoparticles with diameter increasing from 30 to 40 nm with the increase of the thermal treatment temperature. As the SiO$_2$ particles are the finest among the studied particles, also the adsorbed film is smooth and uniform allowing a good individualization of the nanoparticles. The local coalescing tendency that favors the clustering of the smallest particles was prevented by using short adsorption time of NCs dispersed in water on glass slides.

The presence of low amounts of Cu$_{0.6}$Co$_{0.4}$Fe$_2$O$_4$ in SiO$_2$ matrix ($\alpha = 25$%) leads to a slight increase of the nano-particles diameter, but do not influence the surface smoothness and adsorbed film uniformity. The increase of Cu$_{0.6}$Co$_{0.4}$Fe$_2$O$_4$ embedded in the SiO$_2$ matrix highly modifies the adsorbed film surface due to the increase of diameter and roughness. The NCs with $\alpha = 75$% thermally treated at 1200 °C have particles with a diameter of 90 nm and a film roughness of 4.77 nm, being close to the upper nano range. The Cu$_{0.6}$Co$_{0.4}$Fe$_2$O$_4$ ($\alpha = 100$%) thermally treated at 500 °C has round-

shape nanoparticles with a diameter of about 60 nm.

The increase of the thermal treatment temperature to 1200 °C leads to larger particles diameter (100−120 nm) in agreement with the observed crystallinity. The large particles in case of $\alpha = 100$% thermally treated at 1200 °C affects the surface roughness which increases about twenty times compared to $\alpha = 0$%.

The data obtained by XRD and AFM are in good agreement and indicate that the SiO$_2$ matrix is an amorphous phase with small nano-particles (30 nm). Such nanostructure of the matrix assures a good spreading of ferrite nano-particles into the composite and avoids aggregation of the magnetic clusters. The formation of crystalline Co−Cu ferrite is favored by the increase of the annealing temperature. The XRD peaks become more intense and sharper with the increase of the ferrite nano-particles diameter, and the AFM imaging indicate that the ferrite nano-particles are individualized in dispersion.

The determination of specific surface area (SSA) and pore size distribution were successfully performed only for NCs thermally treated at 200 and 500 °C. The N$_2$ adsorption isotherms could not be registered for SiO$_2$ ($\alpha = 0$%) sample heated at 200 °C because the degassing was not possible for this sample, at 100 °C and in vacuum the sample being not stable. For the NCs thermally treated at higher temperatures (800 and 1200 °C), no N$_2$ adsorption-desorption isotherms could be registered indicating that the SSA is below the measurements limit of the instrument (0.5 m^2/g). Only a slight decrease of the surface area was observed for samples annealed at 500 °C compared to those thermally treated at 200 °C, but a drastic decrease was observed for all the samples annealed at higher temperatures. This important decrease of SSA is explained by the collapsing of fine porous structure at high calcination temperatures and was previously reported for silica based porous composites [22] as well as other oxidic porous materials [23]. For NCs thermally treated at both 200 and 500 °C, the isotherms (Fig. 4a and b) are of type IV with hysteresis on the desorption branch [24].

The SSA gradually decreases with increasing Cu$_{0.6}$Co$_{0.4}$Fe$_2$O$_4$ content, the SiO$_2$ ($\alpha = 0$%) sample annealed at 500 °C presenting the highest value (365 m^2/g). The non-embedded Cu$_{0.6}$Co$_{0.4}$Fe$_2$O$_4$ ($\alpha = 100$%) have a significantly smaller value: 27 m^2/g for the sample annealed at 200 °C and 5.6 m^2/g for the one annealed at 500 °C (Fig. 4a). The value of SSA for SiO$_2$ is in good accordance with previously studies [25], while for Cu$_{0.6}$Co$_{0.4}$Fe$_2$O$_4$ is lower than those previously reported for Cu or Co ferrites [26]. A possible explanation for the lower SSA values obtained could be the higher temperature used for thermal treatment. The average pores size is considered to be the size corresponding to the main peak in the pore's size distribution diagram (Fig. 4c and d). There is no significant difference between the pore size distribution for the samples thermally treated at 200 and 500 °C. The pore size distribution diagram (Fig. 4c and d) shows that all materials present a multimodal pore size structure, with the majority of pores having the average pore radius of 10 Å for SiO$_2$ matrix and 25 Å for NCs with higher ferrite content.

These results of SSA measurement for $(Cu_{0.6}Co_{0.4}Fe_2O_4)_{\alpha}(SiO_2)_{100-\alpha}$ NCs are correlated with XRD and AFM results: NCs with higher crystallite size and higher particle size present lower surface area per mass unit, due to the decrease of exposed surface for larger

Table 1
Cu$_{0.6}$Co$_{0.4}$Fe$_2$O$_4$ crystallites size and crystallinity in $(Cu_{0.6}Co_{0.4}Fe_2O_4)_{\alpha}(SiO_2)_{100-\alpha}$.

Thermal treatment	200 °C				500 °C				800 °C				1200 °C			
A	25	50	75	100	25	50	75	100	25	50	75	100	25	50	75	100
D$_C$, nm	−	4	8	15	5	31	43	53	34	43	65	92	45	56	84	110
Degree of crystallinity, %	0	18	34	93	0	35	45	96	15	50	85	98	91	94	97	100

500ºC **800ºC** **1200ºC**
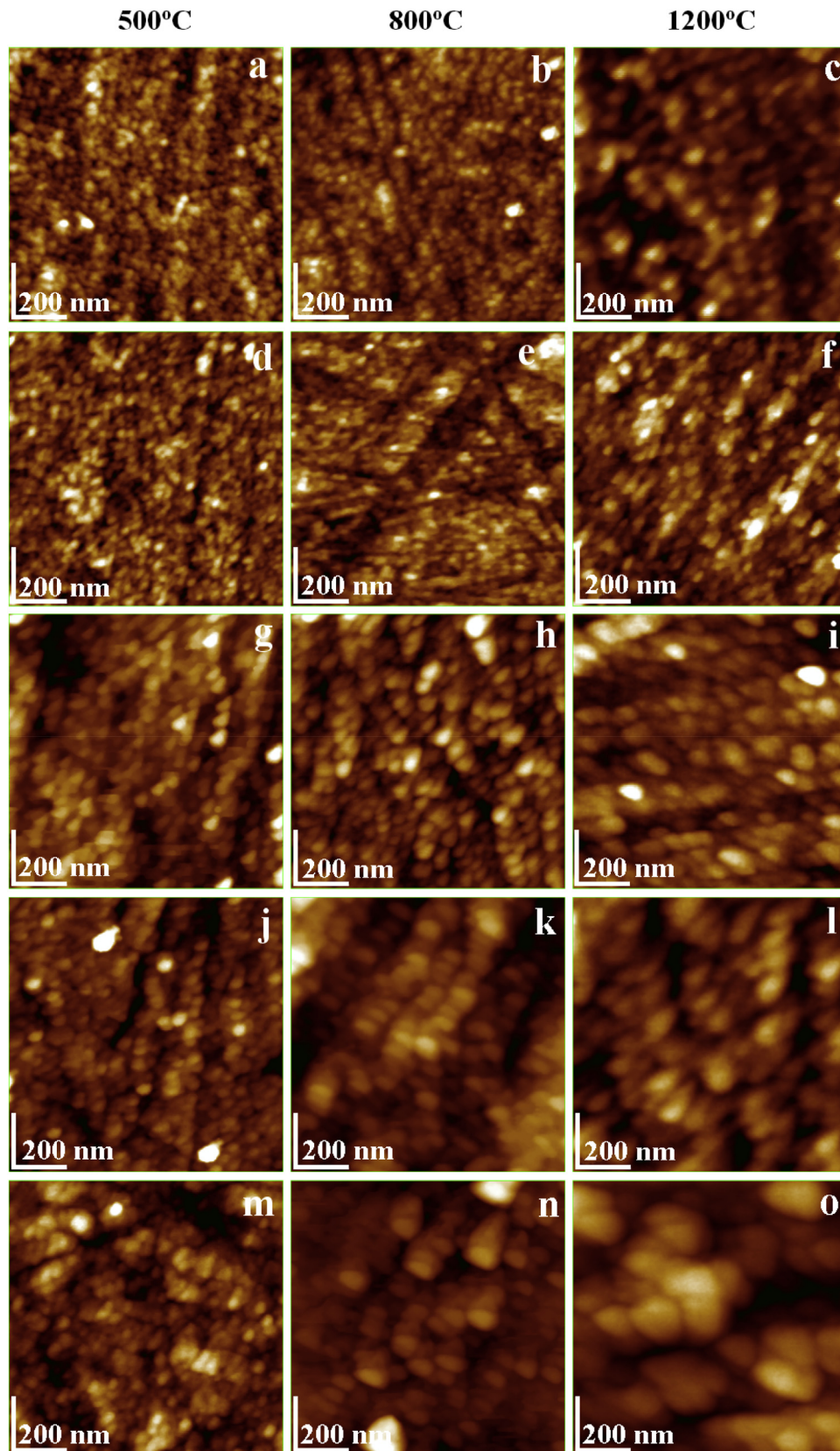
Fig. 2. AFM topographic images of thermally treated $(Cu_{0.6}Co_{0.4}Fe_2O_4)_\alpha(SiO_2)_{100-\alpha}$ α = 0% (a, b, c); α = 25% (d, e, f); α = 50% (g, h, i); α = 75% (j, k, l) and α = 100% (m, n, o).

500°C   **800°C**   **1200°C**

Fig. 3. AFM tridimensional topographic images of thermally treated $(Cu_{0.6}Co_{0.4}Fe_2O_4)_\alpha(SiO_2)_{100-\alpha}$ $\alpha = 0\%$ (a, b, c); $\alpha = 25\%$ (d, e, f); $\alpha = 50\%$ (g, h, i); $\alpha = 75\%$ (j, k, l) and $\alpha = 100\%$ (m, n, o).
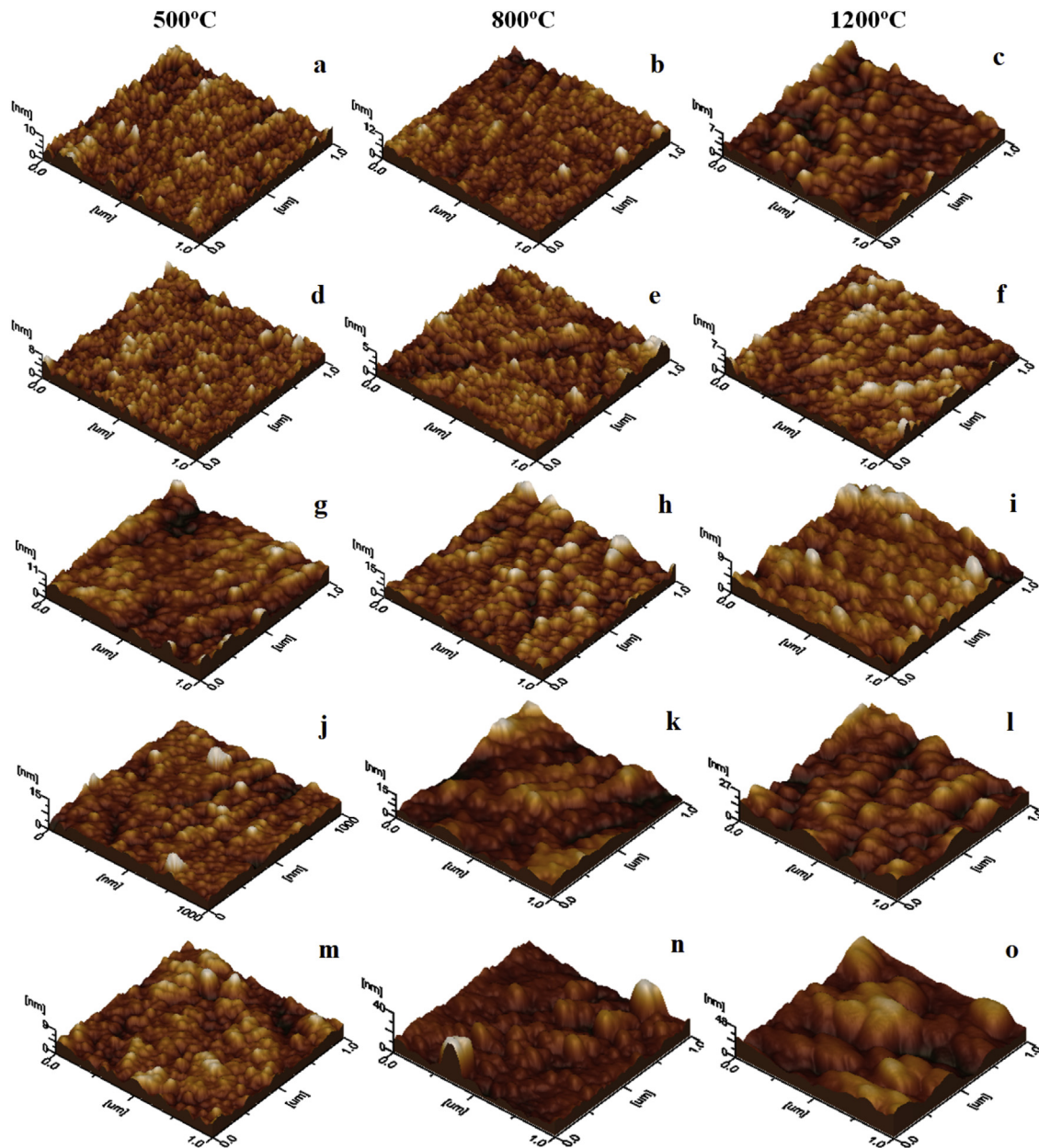
Table 2
$(Cu_{0.6}Co_{0.4}Fe_2O_4)_\alpha(SiO_2)_{100-\alpha}$ particle size, height and roughness measured by AFM.

Thermal treatment	500 °C					800 °C					1200 °C				
α	0	**25**	**50**	**75**	100	0	**25**	50	**75**	100	0	**25**	50	**75**	100
Height, nm	10.0	8.0	11.0	15.0	9.0	12.0	5.0	15.0	15.0	40.0	7.0	7.0	9.0	27.0	48.0
Rq roughness, nm	1.17	0.91	1.53	1.38	1.22	1.21	0.68	1.95	2.07	3.56	0.87	0.89	1.18	3.45	8.04
Particle size,nm	30	33	35	50	60	35	40	50	70	100	40	48	60	90	120

nanoparticles compared to smaller one with similar intrinsic porosity.

The curves of magnetization derivative $(dM/d(\mu_0H))$ vs. applied magnetic field give information about the existing magnetic phases and particle-size distribution. The SiO$_2$ content and the thermal treatment temperature are key parameters to obtain single-phase nano-ferrites with improved magnetic properties. The magnetic hysteresis loops of $(Cu_{0.6}Co_{0.4}Fe_2O_4)_\alpha(SiO_2)_{100-\alpha}$ ($\alpha = 25, 50, 75, 100\%$) thermally treated at 1200 °C are presented in Fig. 5. The saturation magnetization (M_S), remanent magnetization (M_R), coercive field (H_C) and anisotropy constant (K) values, as well as the magnetization derivatives ($dM/d(\mu_0H)$) were calculated from these
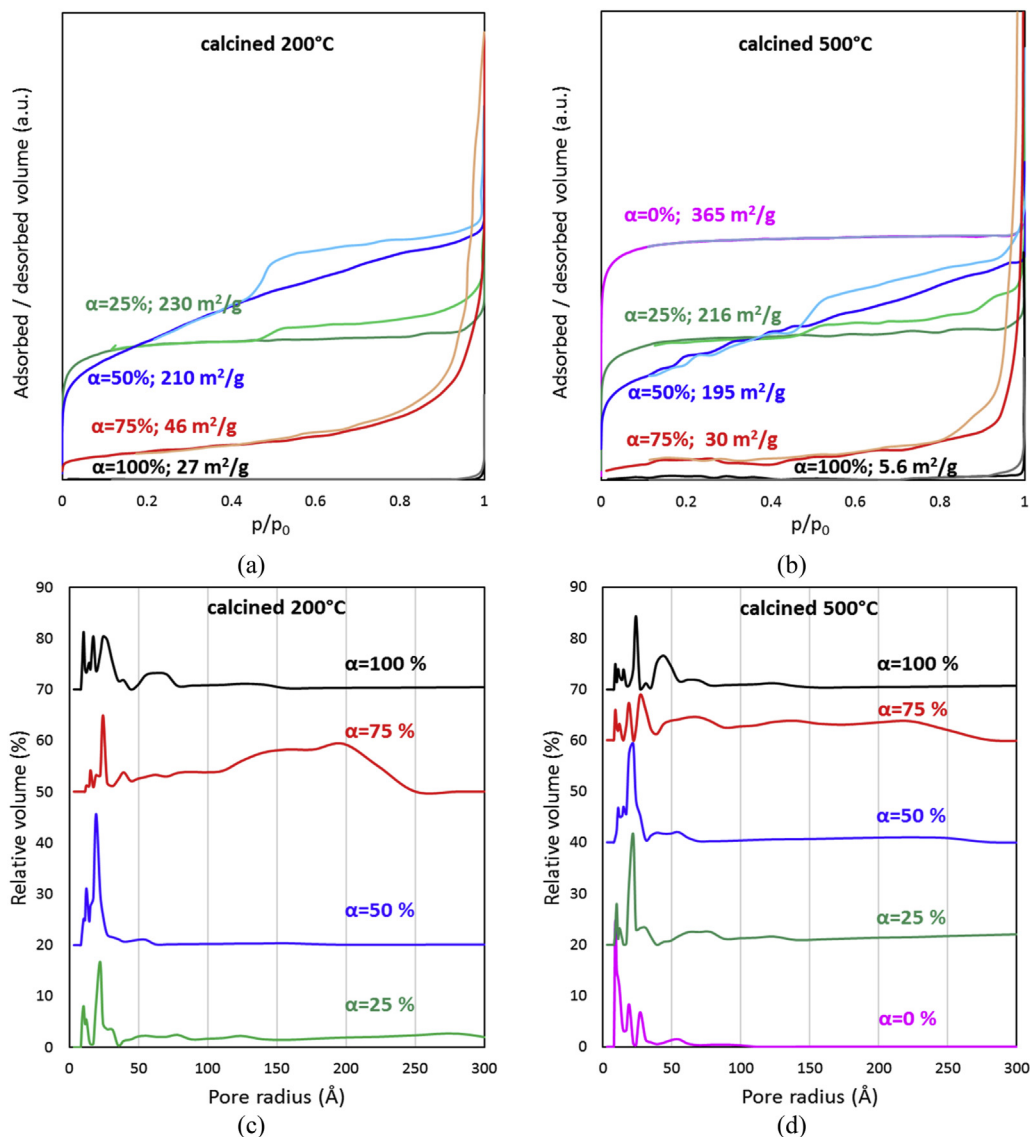
Fig. 4. N_2 adsorption-desorption isotherms (a,b) and pore size distribution (c,d) for $(Cu_{0.6}Co_{0.4}Fe_2O_4)_\alpha(SiO_2)_{100-\alpha}$ thermally treated at 200 and 500 °C.

curves. At low annealing temperatures, the values of the main magnetic parameters were too small in order to investigate the effect of thermal treatment on the magnetic behavior of the samples. As known, the SiO_2 matrix ($\alpha = 0\%$) thermally treated at 1200 °C is diamagnetic and does not have magnetic properties. The highest value of M_S (62.5 emu/g) was found for $Cu_{0.6}Co_{0.4}Fe_2O_4$ ($\alpha = 100\%$) that have also the larger particle sizes as revealed by AFM. The decrease of M_S with decreasing of Cu–Co ferrite content from 41.2 emu/g ($\alpha = 75\%$) to 9.2 emu/g ($\alpha = 25\%$) can be attributed to the effect of SiO_2 matrix. Besides the dilution effect, the magnetic SiO_2 matrix creates disorder effects at the surface of particles, spin canting, pinning of the magnetic moments, broken chemical bonds and influences on the particles size distribution.

The increase of the ferrite content results in the enhancement of M_R from 3.9 emu/g (for $\alpha = 25\%$) to 19 emu/g ($\alpha = 100\%$). The H_C increases with decreasing Cu–Co ferrite content within the SiO_2 matrix from 12.7 kA/m ($\alpha = 100\%$) to 39.9 kA/m ($\alpha = 25\%$). This behavior can be explained by the magnetic domain structure and magneto-crystalline anisotropy. For NCs with $\alpha = 100, 75, 50\%$ the H_c have low values while the maximum value of the magnetization is large, suggesting the presence of large particle sizes and

enhanced magnetic coupling [9,10]. When Cu^{2+} is doped in the Co ferrite structure, less Co^{2+}-Fe^{3+} ions pairs are formed, leading to a lower magnetization value, since Cu^{2+} prefer to occupy the tetrahedral sites and it has a lower magnetic moment than Co^{2+} [21]. The hysteresis loop of cobalt ferrite has a large area with H_C, typical for a hard-magnetic material [9].

The K of the studied nanoparticles was estimated by the method described in our previous work [16–18] based on the hysteresis loops (Fig. 5). The values of K decrease with decreasing $Cu_{0.6}Co_{0.4}$-Fe_2O_4 content in NCs from 0.63×10^{-3} erg/cm^3 ($\alpha = 100\%$) to 0.29×10^{-3} erg/cm^3 ($\alpha = 25\%$).

The magnetic anisotropy of a permanent magnet is characterized mainly by K and is influenced by the crystallographic axes and the type and sizes of the inhomogeneity [9,10]. The $Cu_{0.6}Co_{0.4}Fe_2O_4$ ($\alpha = 100\%$) particles have the highest K and requires a high magnetic field to reach saturation M_S, due to partial magnetic disorder determined by the surface effects on the surfaces of the ferrite particles [9,10]. The increase of H_C with the decreasing ferrite content is related to the particle sizes. As known, the increase of particles size above a critical diameter D_S, results in reducing the H_C of the multi-domain particles [27]. Another contribution to this
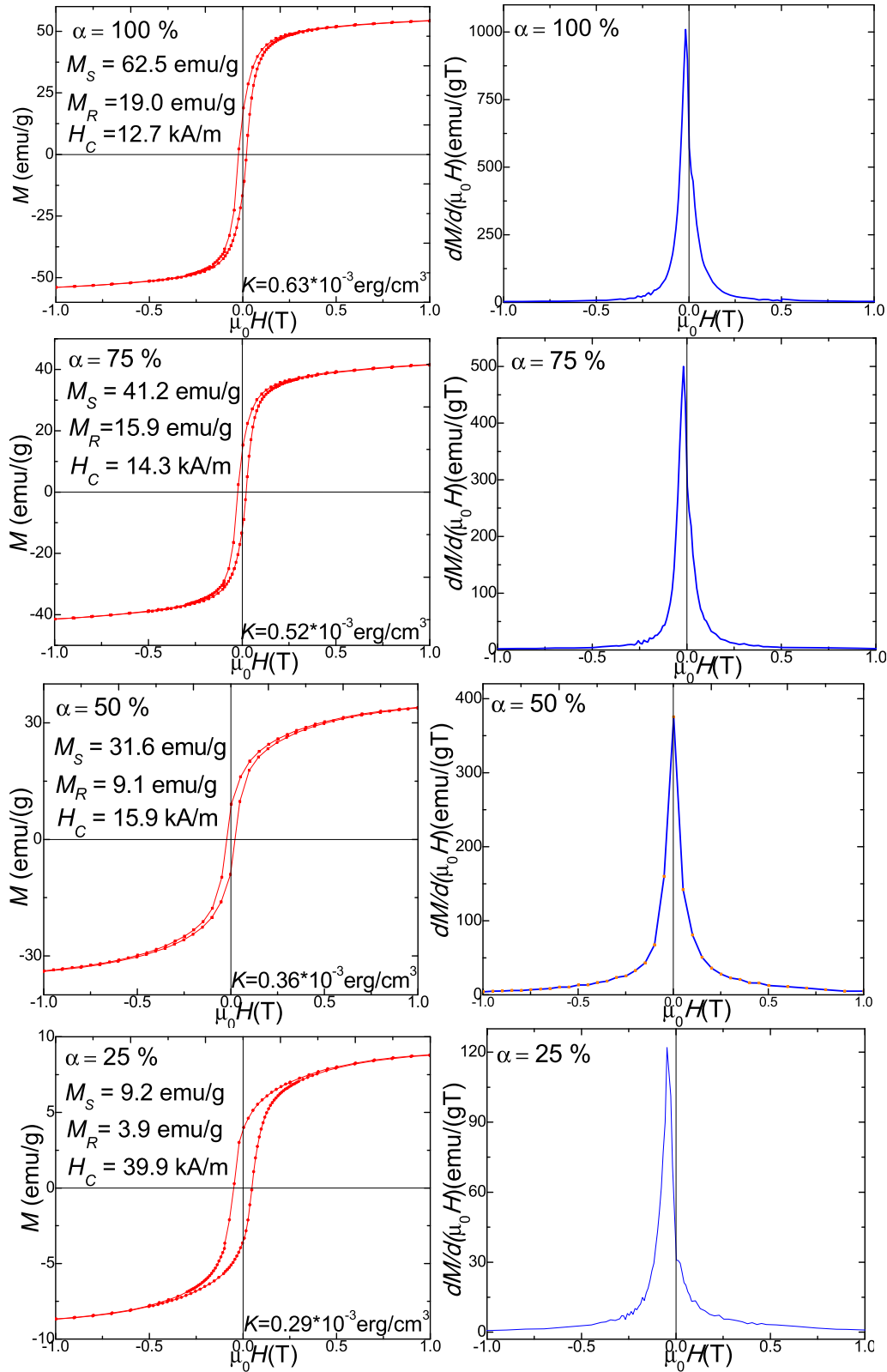
Fig. 5. Magnetic hysteresis loops and magnetization derivative of $(Cu_{0.6}Co_{0.4}Fe_2O_4)_\alpha(SiO_2)_{100-\alpha}$ thermally treated at 1200 °C.

effect can arise from the strain on the surface of the ferrite particles due to the SiO_2 matrix, which hinders the rotation of the magnetic moments from the particle surface [27].

Since particle sizes decrease with increasing SiO_2 content in the NCs, the number of such interfaces increases, enhancing the amount of the magnetic field required to rotate the magnetization.

The curves of magnetization derivative ($dM/d(\mu_0H)$) vs. applied magnetic field (Fig. 5) show only one peak indicating the presence

of a single magnetic phase, for NCs with α = 25-100%. The broad peaks in dM/dH curves suggest large distributions of particle sizes which are related to an increased distribution of the H_C. The peaks width reflects the particle size distribution, while the peak heights and shapes suggests magnetic nanoparticles embedded in amorphous SiO_2 matrix [16–18,28–30].

The obtained results indicated that both the structural and the magnetic properties of the $\alpha Cu_{0.6}Co_{0.4}Fe_2O_4/(100-\alpha)SiO_2$ NCs are strongly affected by the content of SiO_2 amorphous matrix, as well as, by the thermal treatment route used to prepare the samples. Thus, the crystallization temperature, particle size and magnetic behavior may be easily tuned by ferrite embedding in SiO_2 matrix. Furthermore, the combination of the magnetic properties and morphological configuration of the $Cu_{0.6}Co_{0.4}Fe_2O_4/SiO_2$ can be of interest for several technical applications, such as ferrofluids or transformer cores.

4. Conclusions

This work presents a detailed study on the effect of amorphous SiO_2 matrix on the structural and magnetic properties of $\alpha Cu_{0.6}Co_{0.4}Fe_2O_4/(100-\alpha)SiO_2$ NCs (with α = 0, 25, 50, 75 and 100%) obtained under different thermal treatments (200, 500, 800 and 1200 °C). In case of low amounts of Cu–Co ferrite embedded in SiO_2 matrix, secondary crystalline CuO phase appears beside the Cu–Co ferrite, while in samples with high Cu–Co ferrite content embedded in SiO_2 matrix, single-phase crystalline Cu–Co ferrite appears. The non-embedded Cu–Co ferrite displays the highest crystallite size and crystallinity. The crystallite size of $Cu_{0.6}Co_{0.4}Fe_2O_4$ increases with increasing ferrite content in the SiO_2 matrix as follows: 4–15 nm (200 °C), 5–53 nm (500 °C), 34–92 nm (800 °C) and 45–110 nm (1200 °C). The FT-IR spectra confirm the formation of SiO_2 matrix and Cu–Co ferrite. The amorphous SiO_2 matrix has the finest nanoparticles size (30 nm) which assures the refinement of Cu–Co ferrite powders nanostructure. The size of round shaped Cu–Co ferrite nanoparticles decreases with increasing SiO_2 matrix content. The surface roughness and height depend mainly on the particles size and their density in the surface. The SSA gradually increases with increasing SiO_2 content of the NCs and decreases with increasing annealing temperature. Important differences are observed between the SSA of SiO_2 (365 m^2/g annealed at 500 °C) and Cu–Co ferrite (27 m^2/g for the sample dried at 200 °C and 5.6 m^2/g for the sample annealed at 500 °C). For the $(Cu_{0.6}Co_{0.4}Fe_2O_4)_\alpha(SiO_2)_{100-\alpha}$ samples with α = 25, 50, 75%, intermediate values between these two limits were obtained. For the samples thermally treated at high temperatures (800 and 1200 °C), the SSA is very low and couldn't be determined. The mean pore radius of the NCs with ferrite content is 25 Å, similar with the one of non-embedded $Cu_{0.6}Co_{0.4}Fe_2O_4$. The magnetic parameters enhance with increasing $Cu_{0.6}Co_{0.4}Fe_2O_4$ ferrite content in the SiO_2 matrix, as follows M_S from 9.2 to 62.5 emu/g, M_R from 3.9 to 19 emu/g, K from 0.63×10^{-3} to 0.29×10^{-3} erg/cm^3, while the H_C decreases from 0.016 to 0.05 T. When the ferrite is embedded in the SiO_2 matrix, the particle sizes decrease in the nano-range, but the magnetic parameters are altered. Therefore, a compromise between sizes of the NC's and their magnetic properties is necessary for specific technical applications. The obtained NCs could be further developed to obtain soft and thin magnetic films on various solid substrates with tailored properties by varying the matrix/ferrite ratio and by a proper management of adsorption process.

Declaration of competing interest

The authors declare that they have no known competing financial interests or personal relationships that could have appeared to influence the work reported in this paper.

References

[1] M. Hashim, Alimuddin, S. Kumar, B.H. Koo, S.E. Shirsath, E.M. Mohammed, J. Shah, R.K. Kotnala, H.K. Choi, H. Chung, R. Kumar, Structural, electrical and magnetic properties of Co-Cu ferrite nanoparticles, J. Alloys Compd. 518 (2012) 11–18, https://doi.org/10.1016/j.jallcom.2011.12.017.

[2] J. Balavijayalakshmi, N. Suriyanarayanan, R. Jayapraksah, Influence of cooper on the magnetic properties of cobalt ferrite nano particles, Mater. Lett. 81 (2012) 52–54, https://doi.org/10.1016/j.matlet.2012.04.076.

[3] H.M.K. Tedjieukeng, P.K. Tsobnang, R.L. Fomekong, E.P. Etape, P.A. Joy, A. Delcorte, J.N. Lambi, Structural characterization and magnetic properties of undoped and copper-doped cobalt ferrite nanoparticles prepared by the octanoate coprecipitation route at very low dopant concentration, RSC Adv. 8 (2018) 38621–38630, https://doi.org/10.1039/c8ra08532c.

[4] M. Margabandhu, S. Sendhilnathan, S. Senthilkumar, D. Gajalakshmi, Investigation of structural, morphological, magnetic properties and biomedical applications of Cu^{2+} substituted uncoated cobalt ferrite nanoparticles, Braz. Arch. Biol. Technol. 59 (2) (2016), e16161046, https://doi.org/10.1590/1678-4324-2016161046.

[5] K.A. Sampath, T. Himanshu, B. Kevin, S. P Singh, Structural, magnetic and in vitro bioactivity of Co-Cu ferrite and bioglass composite for hyperthermia in bone tissue engineering, Bioceram. Dev. Appl. 6 (1) (2016) 1–7, https://doi.org/10.4172/2090-5025.100091.

[6] B. Chandra Sekhar, G.S.N. Rao, O.F. Caltun, B. Dhana Lakshmi, B. Parvatheeswara Rao, P.S.V. Subba Rao, Magnetic and magnetostrictive properties of Cu substituted Co-ferrites, J. Magn. Magn Mater. 339 (2016) 59–63, https://doi.org/10.1016/j.jmmm.2015.09.028.

[7] L. Wang, M. Lu, Y. Liu, J. Li, M. Liu, H. Lin, The structure, magnetic properties and cation distribution of $Co_{1-x}Mg_xFe_2O_4/SiO_2$ nanocomposites synthesized by sol-gel method, Ceram. Int. 41 (2015) 4176–4181, https://doi.org/10.1016/j.ceramint.2014.12.099.

[8] K. Anu, J. Hemalatha, Magnetic and electrical conductivity studies of zinc doped cobalt ferrite nanofluids, J. Mol. Liquids 284 (2019), https://doi.org/10.1019/j.jmoliq.2019.04.018, 445-153.

[9] M.P. Ghosh, S. Murkherjee, Microstructural, magnetic and hyperfine characterizations of Cu-doped cobalt ferrite nanoparticles, J. Am. Chem. Soc. 102 (2019) 7509–7520, https://doi.org/10.1111/Jace.16687.

[10] S.M. Ansari, S.R. Suryawanshi, M.A. More, D. Sen, Y.D. Kolekar, C.V. Ramana, Field emission properties of nano-structured cobalt ferrite ($CoFe_2O_4$) synthesized by low-temperature chemical method, Chem. Phys. Lett. 701 (2018) 151–156, https://doi.org/10.1016/j.cplett.2018.04.027.

[11] P. Arevalo-Cid, J. Isasi, F. Martin-Hernandez, Comparative study of core-shell nanostructures based on amino-functionalized $Fe_3O_4@SiO_2$ and $CoFe_2O_4@SiO_2$ nanocomposites, J. Alloys Compd. 766 (2018) 609–618, https://doi.org/10.1016/j.jallcom.2018.06.246.

[12] M.A. Dar, D. Varshney, Effect of d-block element Co^{2+} substitution on structural, Mössbauer and dielectric properties of spinel copper ferrite, J. Magn. Magn Mater. 436 (2017) 101–112, https://doi.org/10.1016/j.jmmm.2017.04.046.

[13] S. Azimi, Sol-gel synthesis and structural characterization of nano-thiamine hydrochloride structure, ISRN Nanotechnology (2013) 1–4, https://doi.org/10.1155/2013/815071, ID 815071.

[14] S. Esposito, "Traditional" sol-gel chemistry as a powerful tool for the preparation of supported metal and metal oxide catalysts, Materials 12 (2019) 668, https://doi.org/10.3390/ma12040668.

[15] M. Răileanu, M. Crişan, C. Petrache, D. Crişan, A. Jitianu, M. Zaharescu, D. Predoi, V. Kuncser, G. Filoti, Sol-gel Fe_xO_y – SiO_2 nanocomposites, Rom. J. Phys. 50 (5–6) (2004) 595–606.

[16] M. Stefanescu, M. Stoia, C. Caizer, T. Dippong, P. Barvinski, Preparation of $Co_xFe_{3-x}O_4$ nanoparticles by thermal decomposition of some organo-metallic precursors, J. Therm. Anal. Calorim. 97 (2009) 245–250, https://doi.org/10.1007/s10973-009-0250-x.

[17] T. Dippong, D. Toloman, E.-A. Levei, O. Cadar, A. Mesaros, A possible formation mechanism and photocatalytic properties of $CoFe_2O_4/PVA$-SiO_2 nanocomposites, Thermochim. Acta 666 (2018) 103–115, https://doi.org/10.1016/j.tca.2018.05.021.

[18] T. Dippong, E.A. Levei, O. Cadar, F. Goga, Thermal behavior of Ni, Co and Fe succinates embedded in silica matrix, J. Therm. Anal. Calorim. 136 (2019)

1587−1596, https://doi.org/10.1007/s10973-019-08117-8.

[19] T. Dippong, O. Cadar, E.A. Levei, I.G. Deac, Microstructure, porosity and magnetic properties of $Zn_{0.5}Co_{0.5}Fe_2O_4/SiO_2$ nanocomposites prepared by sol-gel method using different polyols, J. Magn. Magn Mater. 498 (2020) 166168, https://doi.org/10.1016/j.jmmm.2019.166168.

[20] Joint Committee on Powder Diffraction Standards-International Center for Diffraction Data, 1999.

[21] R.K. Singh, B.C. Rai, K. Prasad, Synthesis and characterization of copper substituted cobalt ferrite nanoparticles, Intern. J. Adv. Mater. 3 (2) (2012) 71−76.

[22] J. Ma, J. Chu, L. Qiang, J. Xue, Effect of different calcination temperatures on the structural and photocatalytic performance of $Bi-TiO_2/SBA-15$, Int. J. Photoenergy (2013) (2013), 875456, https://doi.org/10.1155/2013/875456.

[23] C. Sivaraj, C. Contescu, J.A. Schwarz, Effect of calcination temperature of alumina on the adsorption/impregnation of Pd(II) compounds, J. Catal. 132 (1991) 422−431, https://doi.org/10.1016/0021-9517(91)90159-2.

[24] K.S.W. Sing, D.H. Everett, R.A.W. Haul, L. Moscou, R.A. Pierotti, J. Rouquerol, T. Siemieniewska, Physical and biophysical chemistry division commission on colloid and surface chemistry including catalysis, Pure Appl. Chem. 57 (1985) 603−619, https://doi.org/10.1351/pac198557040603.

[25] Z. Liu, J. Zhu, C. Peng, T. Wakihara, T. Okubo, Continous flow synthesis of ordered porous materials: from zeolites to metal-organic frameworks and mesoporous silica, React. Chem, Eng. 4 (2019) 1699−1720, https://doi.org/10.1039/C9RE00142E.

[26] B.I. Kharisov, H.V. Rasika Dias, Oxana V. Kharissova, Mini-review: ferrite nanoparticles in the catalysis, Arab. J. Chem. 12 (2019) 1234−1246, https://doi.org/10.1016/j.arabjc.2014.10.049.

[27] B.D. Cullity, C.D. Graham, Introduction to Magnetic Materials, John Wiley & Sons, Inc., Hoboken, New Jersey, 2009, p. 359.

[28] E.H. Feutrill, P.G. McCormick, R. Street, Magnetization behaviour in exchange-coupled $Sm_2Fe_{14}Ga_3C_2/\alpha$-Fe, J. Phys. D Appl. Phys. 29 (1996) 2320−2326.

[29] M. Ziese, A. Setzer, I. Vrejoiu, B.I. Birajdar, B.J. Rodriguez, D. Hesse, Structural, magnetic, and electric properties of $La_{0.7}Sr_{0.3}MnO_3/PbZr_xTi_{1-x}O_3$ heterostructures, J. Appl. Phys. 104 (2008), 063908, https://doi.org/10.1063/1.2980322.

[30] V. Pop, S. Gutoiu, E. Dorolti, O. Isnard, I. Chicinas, The influence of short time heat treatment on the structural and magnetic behaviour of $Nd_2Fe_{14}B/\alpha$-Fe nanocomposite obtained by mechanical milling, J. Alloys Compd. 509 (2011) 9964−9969, https://doi.org/10.1016/j.jallcom.2011.08.002.